

Article

N₂O Direct Dissociation over Mg_xCe_yCo_{1-x-y}Co₂O₄ Composite Spinel Metal Oxide

Ning Liu ^{1,2}, Ping Chen ¹, Yingxia Li ¹ and Runduo Zhang ^{1,*}

¹ State Key Laboratory of Chemical Resource Engineering, Beijing University of Chemical Technology, Beijing 100029, China; liuning@mail.buct.edu.cn (N.L.); 2014210021@mail.buct.edu.cn (P.C.); Liyx@mail.buct.edu.cn (Y.L.)

² Changzhou Institute of Advanced Materials, Beijing University of Chemical Technology, Changzhou 213164, China

* Correspondence: zhangrd@mail.buct.edu.cn; Tel.: +86-010-6441-2054

Academic Editors: Enrique Rodríguez-Castellón, Agustín Bueno-López and Elisa Moretti

Received: 25 November 2016; Accepted: 23 December 2016; Published: 1 January 2017

Abstract: A series of Mg- and/or Ce-doped Co₃O₄ (Mg_xCo_{1-x}Co₂O₄ Ce_xCo_{1-x}Co₂O₄, Mg_xCe_yCo_{1-x-y}Co₂O₄) composite spinel metal-oxide catalyst was prepared by a coprecipitation method and evaluated for N₂O direct decomposition. The activity measurement results suggest that Mg_{0.025}Ce_{0.05}Co_{0.925}Co₂O₄ with a Mg/Ce mole ratio of 0.5 exhibited the highest N₂O conversion activity, achieving 100% N₂O conversion at $T = 250$ °C (35 vol % N₂O balanced by He, gas hourly space velocity (GHSV) = 30,000 h⁻¹). Characterizations using X-ray diffraction (XRD), Brunauer–Emmett–Teller method (BET), hydrogen temperature-programmed reduction (H₂-TPR), and X-ray photoelectron spectroscopy (XPS) reveal that there were three main reasons for the excellent catalytic behavior of Mg_{0.025}Ce_{0.05}Co_{0.925}Co₂O₄: (a) Mg and Ce co-doping could reduce the grain size of composite spinel metal oxide, which thereby significantly increased the BET specific surface area of Mg_{0.025}Ce_{0.05}Co_{0.925}Co₂O₄ (111.2 g·m⁻² with respect to that of 32.5 g·m⁻² for Co₃O₄); (b) Mg and Ce co-doping could improve the redox ability of Mg_{0.025}Ce_{0.05}Co_{0.925}Co₂O₄, including reductions of Co³⁺ → Co²⁺ and Co²⁺ → Co⁰; and (c) Mg and Ce co-doping not only could improve the migration ability of surface atomic O, but also could increase the concentrations of surface atomic O.

Keywords: N₂O catalytic decomposition; composite spinel metal oxide; Mg_xCe_yCo_{1-x-y}Co₂O₄

1. Introduction

Nitrous oxide (N₂O) is one kind of colorless and weakly sweet gas, which was considered to be a nonpolluting gas for a long time, due to its harmlessness to human beings [1,2]. Recently, people have developed a much more profound understanding of N₂O: (a) N₂O has a global warming potential (GWP) about 310 times higher than that of CO₂, which contributes to 6% of the global greenhouse effect [3]; (b) N₂O can damage the ozone layer through a cyclic chain reaction system; (c) N₂O has a very long atmospheric lifetime, nearly 150 years, as it is hard to decompose. In light of this, N₂O emissions in some European countries have been bounded by the regulation of “Kyoto Protocol” [4]. However, the N₂O content in the atmosphere is still rising. It has been mainly released from chemical industry processes, for example, adipic acid and nitric acid industry [5]. In addition to that, with the rapid increase of the numbers of vehicles, the N₂O emitted from automobile engines also contributes to the increasing content of N₂O in the atmosphere. Therefore, N₂O emission control has become a global issue to protect our living environment.

Commonly, there are three ways for N₂O abatement, including thermal pyrolysis [6], selective catalytic reduction [7–9], and direct decomposition [10–17]. The advantage of thermal pyrolysis is that it does not need catalyst. However, the high treatment temperature of ~800 °C not only

can cause substantial energy consumption, but can also generate large amounts of NO_x , resulting in a second air pollution problem. In addition to that, N_2O decomposition ($de\text{N}_2\text{O}$) efficiency of thermal pyrolysis method is low, which cannot meet increasingly strict legislations. As for the selective catalytic reduction method, its treatment temperature is much lower than that of the thermal pyrolysis method; however, further addition of reductant, hydrocarbons, and ammonia, for example, greatly increases the $de\text{N}_2\text{O}$ expense.

As for the direct decomposition method, it can directly decompose the N_2O into N_2 and O_2 at relatively low temperatures. Moreover, it does not need any additional reductant. Therefore, the direct decomposition method serves as a candidate method for N_2O abatement. The catalysts involved in N_2O direct decomposition include a noble metal catalyst [10], metal-oxide catalyst [11–15], and zeolite catalyst [16–18]. Noble metal catalysts are expensive and can be readily contaminated by the coexistence of NO gas, which greatly hinders their practical application. Zeolite catalysts—especially Fe-ZSM-5, Fe-BEA, and Fe-FER—have been widely investigated for N_2O direct decomposition due to their excellent N_2O conversion activity; however, relatively low hydrothermal stability constitutes one of their biggest problems, especially during practical applications.

A type of metal-oxide catalyst, cobalt spinel (Co_3O_4) [11,13–15], has been proposed to be a promising candidate for N_2O abatement, due to its excellent $de\text{N}_2\text{O}$ activity (achieving 100% N_2O at $T = 300\text{ }^\circ\text{C}$) and high thermal stability. As reported [14], the N_2O decomposition over cobalt spinel is a classic redox reaction, involving N_2O molecule activation by electron transfer from a cobalt (II) cation to a N_2O molecule (Equation (1)). The produced oxygen species can migrate to the surface of the catalyst and finally recombine with each other, forming an O_2 molecule (Equation (2)), which closes the catalytic cycle.



According to the literature report, the specific surface area and catalytic activity can be effectively improved by doping Mg into Co_3O_4 [15]. Meanwhile, ceria (CeO_2), which is commonly used as a catalytic support, possesses good oxygen storage capacity and thermal stability, which can also effectively enhance the $de\text{N}_2\text{O}$ catalytic activity of Co_3O_4 [14]. Therefore, in the present work, a series of single Mg- or Ce-doped Co_3O_4 ($\text{Mg}_x\text{Co}_{1-x}\text{Co}_2\text{O}_4$ or $\text{Ce}_x\text{Co}_{1-x}\text{Co}_2\text{O}_4$, respectively) and Mg, Ce co-doped Co_3O_4 ($\text{Mg}_x\text{Ce}_y\text{Co}_{1-x-y}\text{Co}_2\text{O}_4$) spinel composite metal-oxide catalyst were prepared by a coprecipitation method, which was further evaluated for N_2O direct decomposition. The effects of Mg-, Ce-doping were thereafter analyzed by various characterizations using X-ray diffraction (XRD), Brunauer–Emmett–Teller method (BET), hydrogen temperature-programmed reduction (H_2 -TPR), and X-ray photoelectron spectroscopy (XPS) to give detailed information on the crystal structure, grain size, specific surface area, redox ability, and surface chemical state of the prepared catalyst samples. Through the investigation of present work, a promising N_2O direct decomposition candidate with high activity is proposed.

2. Results and Discussion

2.1. XRD and BET Results

XRD was conducted for samples of $\text{Mg}_{0.2}\text{Co}_{0.8}\text{Co}_2\text{O}_4$, $\text{Ce}_{0.05}\text{Co}_{0.95}\text{Co}_2\text{O}_4$, and $\text{Mg}_{0.025}\text{Ce}_{0.05}\text{Co}_{0.925}\text{Co}_2\text{O}_4$, in order to investigate the effects of Mg-, Ce-doping on the crystal structure of Co_3O_4 . The related XRD patterns are profiled in Figure 1, wherein the XRD pattern of Co_3O_4 was taken as a reference. It can be found that all the samples exhibited the characteristic diffraction peaks of the Co_3O_4 spinel phase (18.9° , 31.3° , 36.8° , 44.8° , 55.7° , 59.6° , 65.2° , JCPDS 80-1541). However, after Mg- and Ce-doping, the diffraction peaks significantly decreased, especially at 36.8° , which reveals that the grain size of Co_3O_4 decreased after Mg-, Ce-doping. As shown in Table 1,

the calculated grain sizes (Scherrer equation of Equation (3)) decreased in the order of $\text{Co}_3\text{O}_4 > \text{Mg}_{0.2}\text{Co}_{0.8}\text{Co}_2\text{O}_4 > \text{Ce}_{0.05}\text{Co}_{0.95}\text{Co}_2\text{O}_4 > \text{Mg}_{0.025}\text{Ce}_{0.05}\text{Co}_{0.925}\text{Co}_2\text{O}_4$. Similar findings were also observed by Xue et al. [13] and Stelmachowski et al. [15]. It was explained in [15] that introduction of Mg, Al into Co_3O_4 spinel could increase Co_3O_4 spinel lattice constant a , but decreased another lattice constant u (defining the position of oxygen anions in the spinel lattice), which led to final decreasing of the Co–O bond lengths in both the tetrahedral and octahedral units. Therefore, it could be deduced that the decreasing crystallization of prepared Mg-, and/or Ce-doped Co_3O_4 was due to the special interaction between doped metals (Mg, Ce), with Co located at octahedral and tetrahedral units.

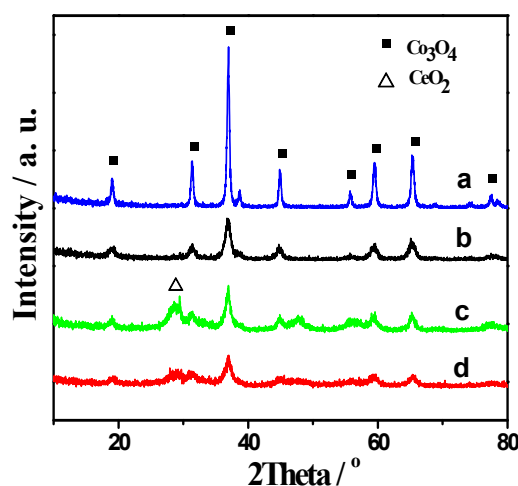


Figure 1. X-ray diffraction (XRD) patterns of $\text{Mg}_x\text{Ce}_y\text{Co}_{1-x-y}\text{Co}_2\text{O}_4$ composite spinel metal oxide: (a) Co_3O_4 ; (b) $\text{Mg}_{0.2}\text{Co}_{0.8}\text{Co}_2\text{O}_4$; (c) $\text{Ce}_{0.05}\text{Co}_{0.95}\text{Co}_2\text{O}_4$; (d) $\text{Mg}_{0.025}\text{Ce}_{0.05}\text{Co}_{0.925}\text{Co}_2\text{O}_4$.

Table 1. Brunauer–Emmett–Teller (BET) specific surface area and crystal size of the catalysts.

Catalysts	BET Specific Surface Area ($\text{m}^2\cdot\text{g}^{-1}$)	Crystal Size (nm)
Co_3O_4	32.5	22.4
$\text{Mg}_{0.2}\text{Co}_{0.8}\text{Co}_2\text{O}_4$	77.8	14.6
$\text{Ce}_{0.05}\text{Co}_{0.95}\text{Co}_2\text{O}_4$	106.5	11.8
$\text{Mg}_{0.025}\text{Ce}_{0.05}\text{Co}_{0.925}\text{Co}_2\text{O}_4$	111.2	10.1

The specific surface areas of Co_3O_4 , $\text{Mg}_{0.2}\text{Co}_{0.8}\text{Co}_2\text{O}_4$, $\text{Ce}_{0.05}\text{Co}_{0.95}\text{Co}_2\text{O}_4$, and $\text{Mg}_{0.025}\text{Ce}_{0.05}\text{Co}_{0.925}\text{Co}_2\text{O}_4$ are also listed in Table 1. It can be found that compared with pure Co_3O_4 ($32.5 \text{ m}^2\cdot\text{g}^{-1}$), a significant increase of the specific surface area was observed for Mg-, Ce-doped Co_3O_4 spinel metal oxides ($111.2 \text{ m}^2\cdot\text{g}^{-1}$ for $\text{Mg}_{0.025}\text{Ce}_{0.05}\text{Co}_{0.925}\text{Co}_2\text{O}_4$). Meanwhile, the increasing order of BET surface area was consistent with the decreasing order of grain size: $\text{Co}_3\text{O}_4 < \text{Mg}_{0.2}\text{Co}_{0.8}\text{Co}_2\text{O}_4 < \text{Ce}_{0.05}\text{Co}_{0.95}\text{Co}_2\text{O}_4 < \text{Mg}_{0.025}\text{Ce}_{0.05}\text{Co}_{0.925}\text{Co}_2\text{O}_4$. This indicates that the Mg- and Ce-doping could reduce the grain size of Co_3O_4 , which consequently resulted in further increases of the related specific surface area.

2.2. H_2 -TPR

In this section, we describe the influence of Mg-, Ce-doping on the redox ability of Co_3O_4 ($\text{Co}^{3+} \rightarrow \text{Co}^{2+}$ and $\text{Co}^{2+} \rightarrow \text{Co}^0$), as studied by H_2 -TPR, with the results depicted in Figure 2. Two reduction peaks, respectively labeled as PH_2 -I ($250\text{--}350 \text{ }^\circ\text{C}$) and PH_2 -II ($360\text{--}480 \text{ }^\circ\text{C}$), were clearly observed for all investigated samples shown in Figure 2. PH_2 -I represents H_2 reduction of Co_3O_4 to CoO ($\text{Co}^{3+} \rightarrow \text{Co}^{2+}$) and PH_2 -II represents H_2 reduction of CoO to Co^0 ($\text{Co}^{2+} \rightarrow \text{Co}^0$). As noted, there also existed a third reduction peak for the samples of $\text{Ce}_{0.05}\text{Co}_{0.95}\text{Co}_2\text{O}_4$ and $\text{Mg}_{0.025}\text{Ce}_{0.05}\text{Co}_{0.925}\text{Co}_2\text{O}_4$ at $T = 550 \text{ }^\circ\text{C}$, which was probably related to the H_2 reduction of CeO_x [19].

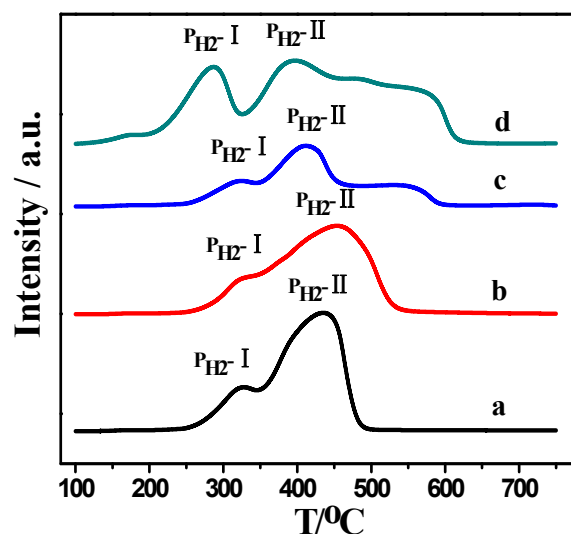


Figure 2. Hydrogen temperature-programmed reduction (H_2 -TPR) profiles of $Mg_xCe_yCo_{1-x-y}Co_2O_4$ composite metal oxides: (a) Co_3O_4 ; (b) $Mg_{0.2}Co_{0.8}Co_2O_4$; (c) $Ce_{0.05}Co_{0.95}Co_2O_4$; (d) $Mg_{0.025}Ce_{0.05}Co_{0.925}Co_2O_4$. PH_2 -I: H_2 reduction of Co_3O_4 to CoO ; PH_2 -II: H_2 reduction of CoO to Co^0 .

In comparison with the H_2 reduction profile of Co_3O_4 (Figure 2a), a much broader reduction peak located at PH_2 -II was observed for $Mg_{0.2}Co_{0.8}Co_2O_4$ (Figure 2b). This implies that the single Mg-doping could increase the Co^{2+} content on $Mg_{0.2}Co_{0.8}Co_2O_4$. It was reported that Co^{2+} oxidation by N_2O to Co^{3+} was the rate-determining step during N_2O direct dissociation over Co_3O_4 [20]. Therefore, in the present work, the increasing amount of Co^{2+} of $Mg_{0.2}Co_2O_4$ is correlated with its superior deN_2O activity with respect to that of pure Co_3O_4 (as will be described later). Different from the effect of Mg-doping, Ce-doping resulted in the reduction peak of PH_2 -II being shifted to much lower temperature ($Ce_{0.05}Co_{0.95}Co_2O_4$ of Figure 2c). This finding implies that the single Ce-doping could increase the redox ability of Co^{2+} ($Co^{2+} \rightarrow Co^0$), which can also well explain the much higher deN_2O activity of $Ce_{0.05}Co_{0.95}Co_2O_4$ versus pure Co_3O_4 . As shown in Figure 2d ($Mg_{0.025}Ce_{0.05}Co_{0.925}Co_2O_4$), when Mg and Ce were simultaneously doped into the Co_3O_4 , the reduction peaks of PH_2 -I and PH_2 -II all moved to the lowest temperature with respect to other samples. This reveals that the co-doping of Mg and Ce on Co_3O_4 could greatly improve the redox ability of Co_3O_4 (both $Co^{3+} \rightarrow Co^{2+}$ and $Co^{2+} \rightarrow Co^0$). In addition to that, according to the literature reports [21,22], the reduction of $Co^{3+} \rightarrow Co^{2+}$ was correlated with the oxygen desorption process. The lower the temperature needed for $Co^{3+} \rightarrow Co^{2+}$ reduction, the easier it will be to remove the oxygen. Therefore, the H_2 -TPR of $Mg_{0.025}Ce_{0.05}Co_{0.925}Co_2O_4$ could well explain why it shows the highest deN_2O activity with respect to other metal-doped Co_3O_4 catalysts.

2.3. XPS

As discussed in this section, XPS was employed to investigate the surface chemical states of abovementioned the Mg-, Ce-doped Co_3O_4 composite spinel metal oxides. The related XPS spectra of $Co2p$, $Ce3d$, and $O1s$ are shown in Figure 3A–C, respectively. As shown in Figure 3A, the binding energies of $Co2p_{3/2}$ and $Co2p_{1/2}$ in pure Co_3O_4 were located at 779.45 eV and 794.45 eV, respectively, with a $Co2p_{3/2}$, $Co2p_{1/2}$ spin-orbital splitting energy difference of 15 eV. After the single Mg-doping ($Mg_{0.2}Co_{0.8}Co_2O_4$ in Figure 3A), the related $Co2p_{3/2}$ and $Co2p_{1/2}$ shifted by 0.8 eV to a lower binding energy with respect to that of Co_3O_4 ; however, the difference in spin-orbital splitting energy remains 15 eV. Similar findings were also found for the samples of $Ce_{0.05}Co_{0.95}Co_2O_4$ and $Mg_{0.025}Ce_{0.05}Co_{0.925}Co_2O_4$. The related $Co2p_{3/2}$ and $Co2p_{1/2}$ shifted to lower binding energies by 1.0 and 1.1 eV, respectively; however, the splitting energy difference remained 15 eV. In general, the decrease in the binding energy

of an element means an increase in its outside nucleus electron density, which consequently results in a decreasing of the element valence state. Therefore, the band shift of Co2p to much lower binding energy for Mg-, Ce-doped Co_3O_4 samples implied that the Co^{2+} content increased after Mg-, Ce-doping. This finding was also verified by the peak analysis of $\text{Co}2p_{3/2}$, discussed later. As noted, the increasing of Co^{2+} content means increasing of the O vacancy on the Mg-, Ce-doped samples. Increasing of O vacancy could then facilitate the mobility of atomic O, which was beneficial for the catalytic reaction. Therefore, the $\text{Mg}_{0.025}\text{Ce}_{0.05}\text{Co}_{0.925}\text{Co}_2\text{O}_4$ sample, displaying the largest Co2p band shift (1.1 eV), would be much more active for N_2O decomposition, as verified by the activity measurement study.

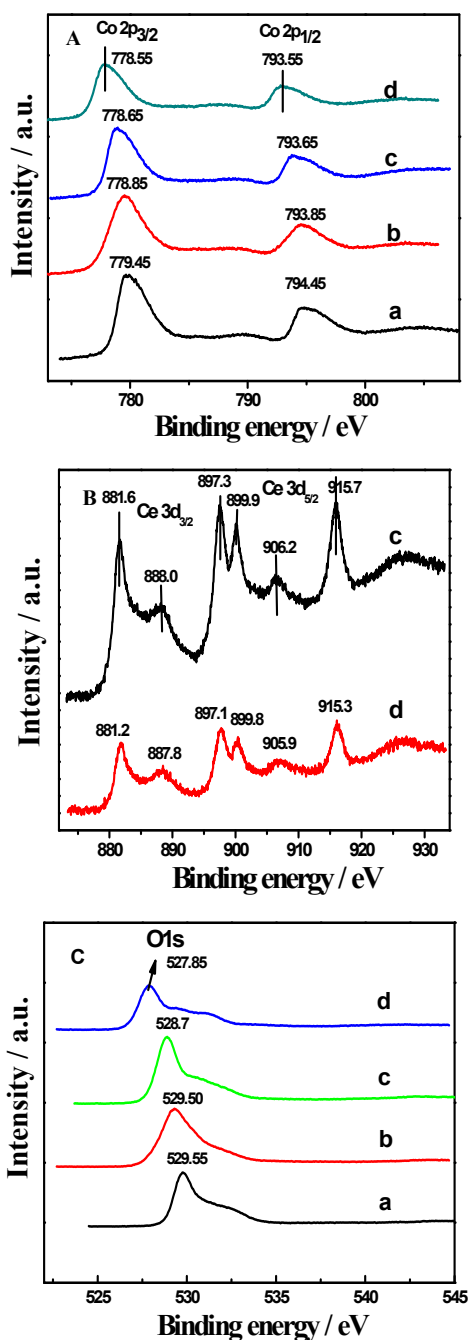


Figure 3. X-ray photoelectron spectroscopy (XPS) spectra of (A) Co2p; (B) Ce3d; and (C) O1s for the composite metal-oxide catalysts: (a) Co_3O_4 ; (b) $\text{Mg}_{0.2}\text{Co}_{0.8}\text{Co}_2\text{O}_4$; (c) $\text{Ce}_{0.05}\text{Co}_{0.95}\text{Co}_2\text{O}_4$; (d) $\text{Mg}_{0.025}\text{Ce}_{0.05}\text{Co}_{0.925}\text{Co}_2\text{O}_4$.

Figure 3B displays Ce 3d_{5/2} and Ce 3d_{3/2} of Ce_{0.05}Co_{0.95}Co₂O₄ and Mg_{0.025}Ce_{0.05}Co_{0.925}Co₂O₄. It can be found that there were no obvious changes in the location of Ce3d for these two samples. This finding indicates that there is no obvious difference in Ce valence state on the surface of Ce_{0.05}Co_{0.95}Co₂O₄ and Mg_{0.025}Ce_{0.05}Co_{0.925}Co₂O₄.

Figure 3C shows O1s of Mg-, Ce-doped Co₃O₄ samples, wherein the O1s of Co₃O₄ was taken as a reference. It can be found that (i) after Mg-, Ce-doping, the O1s of all metal-doped Co₃O₄ composite metal-oxide catalysts shifted to lower binding energy, with respect to that of pure Co₃O₄; (ii) Mg_{0.025}Ce_{0.05}Co_{0.925}Co₂O₄ exhibited the largest O1s band energy shift. As reported [23,24], the decrease of O1s could reduce the interactions between Co and other metal components, which consequently enhance the catalytic activity of Co²⁺. In light of that, Mg_{0.025}Ce_{0.05}Co_{0.925}Co₂O₄ displaying the lowest O1s binding energy can also explain its highest *de*N₂O activity.

Table 2 lists the surface element content of the above-discussed Mg-, Ce-doped Co₃O₄ composite metal-oxide samples, which were measured by XPS. It can be found that after Mg-, Ce-doping, the surface content of atomic Co decreased; however, the content of atomic O increased. This indicates that addition of Mg and Ce into Co₃O₄ could increase concentration of the surface atomic O. As is well known, the surface atomic O exhibits much higher catalytic activity than that of lattice oxygen, especially for the oxidation–reduction reaction system [25]. As noted, the surface atomic O content of Mg_{0.025}Ce_{0.05}Co₂O₄ is highest (76.5%, as seen in Table 2) of all, which constitutes another main factor for its best *de*N₂O catalytic performance.

Table 2. XPS surface atomic percentage.

Sample	Surface Atomic Score Levels (%)				Co ²⁺ /Co ³⁺
	Co	Mg	Ce	O	
Co ₃ O ₄	35.6	0	0	64.4	0.65
Mg _{0.2} Co _{0.8} Co ₂ O ₄	32.7	2.3	0	65.1	0.76
Ce _{0.05} Co _{0.95} Co ₂ O ₄	17.6	0	7.4	74.9	0.91
Mg _{0.025} Ce _{0.05} Co _{0.925} Co ₂ O ₄	17.5	2.4	3.7	76.5	1.11

As stated above, the Co²⁺ content of Me-, Co-doped Co₃O₄ samples increased due to a Co2p band shift to lower values. In order to determine the Co²⁺/Co³⁺ ratio on the surface of prepared Me-, Co-doped Co₃O₄, peak analyses were conducted for Co2p_{3/2}, as shown in Figure 4. According to integral peak areas of Co²⁺, Co³⁺, and total surface Co content, the derived Co²⁺/Co³⁺ values were calculated and are listed in Table 2. It can be clearly seen that the Co²⁺/Co³⁺ value increased in the order of Co₃O₄ < Mg_{0.2}Co_{0.8}Co₂O₄ < Ce_{0.05}Co_{0.95}Co₂O₄ < Mg_{0.025}Ce_{0.05}Co_{0.925}Co₂O₄, suggesting that Mg- and Ce-doping can increased the surface content of Co²⁺, and Mg_{0.025}Ce_{0.05}Co_{0.925}Co₂O₄ possessed the highest Co²⁺ content with respect to other samples.

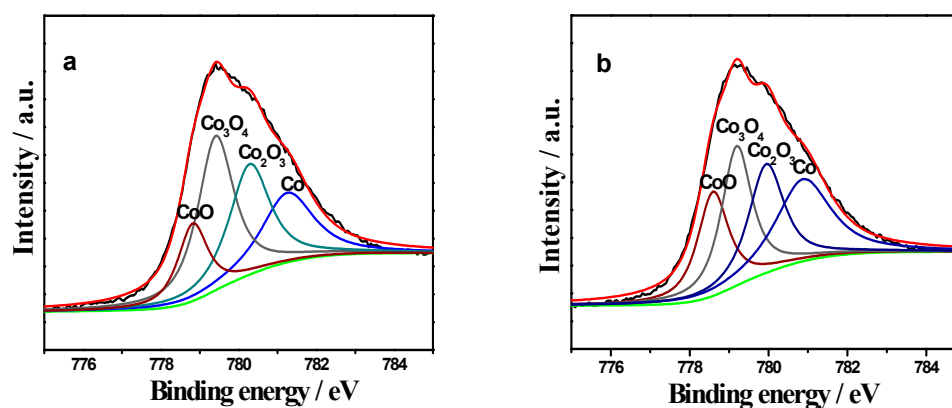


Figure 4. Cont.

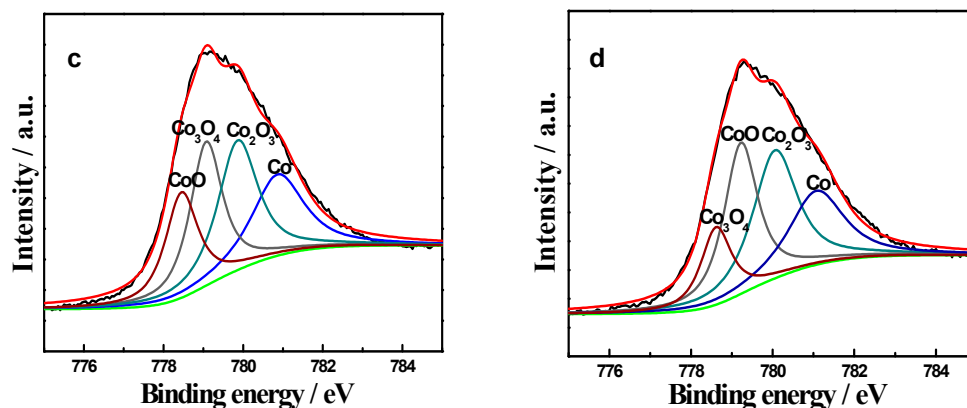


Figure 4. Analysis of $\text{Co}2p_{3/2}$ on composite metal-oxide catalysts (a) Co_3O_4 ; (b) $\text{Mg}_{0.2}\text{Co}_{0.8}\text{Co}_2\text{O}_4$; (c) $\text{Ce}_{0.05}\text{Co}_{0.95}\text{Co}_2\text{O}_4$; (d) $\text{Mg}_{0.025}\text{Ce}_{0.05}\text{Co}_{0.925}\text{Co}_2\text{O}_4$.

2.4. Activity Measurement

Figure 5 displays the activity measurement result of a series of Mg-doped Co_3O_4 samples ($\text{Mg}_x\text{Co}_{1-x}\text{Co}_2\text{O}_4$, $x = 0.2, 0.3, 0.4, 0.5$). It can be found that the $de\text{N}_2\text{O}$ activity of $\text{Mg}_x\text{Co}_{1-x}\text{Co}_2\text{O}_4$ gradually decreased as Mg-doping increased. Among the samples, $\text{Mg}_{0.2}\text{Co}_{0.8}\text{Co}_2\text{O}_4$ exhibited the highest $de\text{N}_2\text{O}$ activity, which could achieve 100% N_2O conversion at $T = 450^\circ\text{C}$. Meanwhile, compared with pure Co_3O_4 (100% N_2O conversion at $T > 500^\circ\text{C}$), much higher $de\text{N}_2\text{O}$ activity was observed for the $\text{Mg}_x\text{Co}_{1-x}\text{Co}_2\text{O}_4$ sample, when the Mg-doping was below 0.4. Therefore, this activity measurement result suggests that a lower amount of Mg-doping is much more preferable.

Figure 6 depicts the activity measurement result of a series of Ce-doped Co_3O_4 samples ($\text{Ce}_x\text{Co}_{1-x}\text{Co}_2\text{O}_4$, $x = 0.03, 0.05, 0.1, 0.2$). The Ce-doping has an obvious promotion effect on $de\text{N}_2\text{O}$ activity, in comparison with that of Co_3O_4 . Among the samples, $\text{Ce}_{0.05}\text{Co}_{0.95}\text{Co}_2\text{O}_4$ exhibited the highest N_2O conversion activity, which could achieve 100% N_2O conversion at $T = 350^\circ\text{C}$. Therefore, through this activity measurement, the optimum doping amount of Ce was chosen to be 0.05.

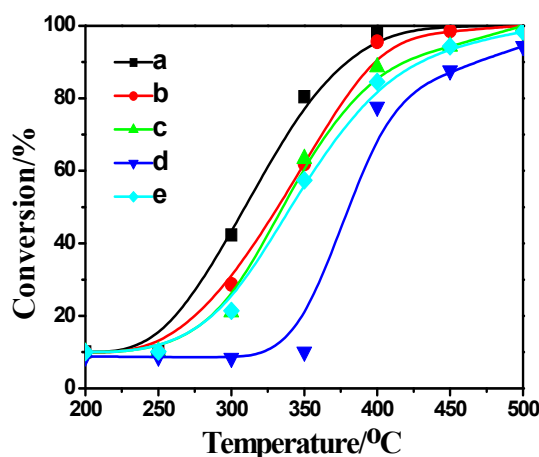


Figure 5. Activity measurement results of N_2O direct dissociation over $\text{Mg}_x\text{Co}_{1-x}\text{Co}_2\text{O}_4$ ($x = 0.2, 0.3, 0.4, 0.5$) composite spinel metal-oxide catalysts. Reaction conditions: $\text{N}_2\text{O}:\text{He} = 35:65$, gas hourly space velocity (GHSV) = $30,000\text{ h}^{-1}$; (a) $\text{Mg}_{0.2}\text{Co}_{0.8}\text{Co}_2\text{O}_4$; (b) $\text{Mg}_{0.3}\text{Co}_{0.7}\text{Co}_2\text{O}_4$; (c) $\text{Mg}_{0.4}\text{Co}_{0.6}\text{Co}_2\text{O}_4$; (d) $\text{Mg}_{0.5}\text{Co}_{0.5}\text{Co}_2\text{O}_4$; (e) Co_3O_4 .

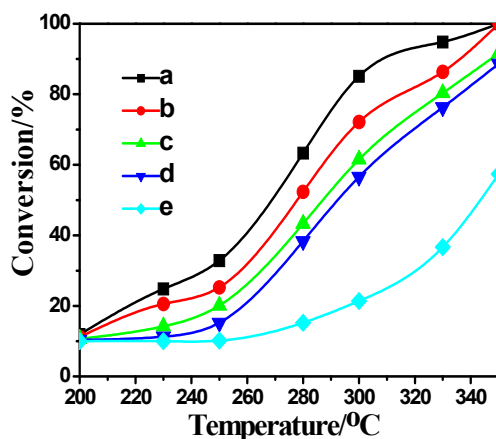


Figure 6. Activity measurement results of N_2O direct dissociation over $\text{Ce}_x\text{Co}_{1-x}\text{Co}_2\text{O}_4$ ($x = 0.03, 0.05, 0.1, 0.2$) composite spinel metal-oxide catalysts. Reaction conditions: $\text{N}_2\text{O}:\text{He} = 35:65$, $\text{GHSV} = 30,000 \text{ h}^{-1}$; (a) $\text{Ce}_{0.05}\text{Co}_{0.95}\text{Co}_2\text{O}_4$; (b) $\text{Ce}_{0.03}\text{Co}_{0.97}\text{Co}_2\text{O}_4$; (c) $\text{Ce}_{0.1}\text{Co}_{0.9}\text{Co}_2\text{O}_4$; (d) $\text{Ce}_{0.2}\text{Co}_{0.8}\text{Co}_2\text{O}_4$; (e) Co_3O_4 .

Based on the above activity measurement results, it can be concluded that the single Mg- or Ce-doping could efficiently improve N_2O activity of the Co_3O_4 spinel catalyst, where: (i) decreasing Mg-doping content is beneficial for improving deN_2O activity; and (ii) the optimum Ce-doping content is 0.05. In light of this, a series of Mg and Ce co-doping of Co_3O_4 ($\text{Mg}_x\text{Ce}_y\text{Co}_{1-x-y}\text{Co}_2\text{O}_4$) was further prepared and evaluated for N_2O direct decomposition, as shown in Figure 7. Ce-loading was chosen to be 0.05 ($y = 0.05$), while Mg-loading varied from 0.015 to 0.15 ($x = 0.015, 0.025, 0.05, 0.1, 0.15$). It can be found that, except for $\text{Mg}_{0.15}\text{Ce}_{0.05}\text{Co}_{0.8}\text{Co}_2\text{O}_4$, $\text{Mg}_x\text{Ce}_y\text{Co}_{1-x-y}\text{Co}_2\text{O}_4$ samples exhibit excellent deN_2O activity, achieving $T_{90} < 300 \text{ }^\circ\text{C}$. Among them, $\text{Mg}_{0.025}\text{Ce}_{0.05}\text{Co}_{0.925}\text{Co}_2\text{O}_4$, with a Mg/Ce ratio of 0.5, shows the best N_2O conversion activity, which could achieve 100% N_2O conversion at $T = 250 \text{ }^\circ\text{C}$. This indicates that the co-doping of Mg and Ce into Co_3O_4 could indeed improve the deN_2O activity, and the best doping content of these samples was $\text{Mg}_{0.025}\text{Ce}_{0.05}\text{Co}_{0.925}\text{Co}_2\text{O}_4$ with a Mg/Ce mole ratio of 0.5. In addition to that, the long lifetime (30 h) deN_2O activity measurement was further conducted for the best-performing $\text{Mg}_{0.025}\text{Ce}_{0.05}\text{Co}_{0.925}\text{Co}_2\text{O}_4$ sample at $T = 250 \text{ }^\circ\text{C}$, as shown in Figure 8. It can be found that the prepared sample exhibited stable deN_2O activity, implying excellent durability of this sample.

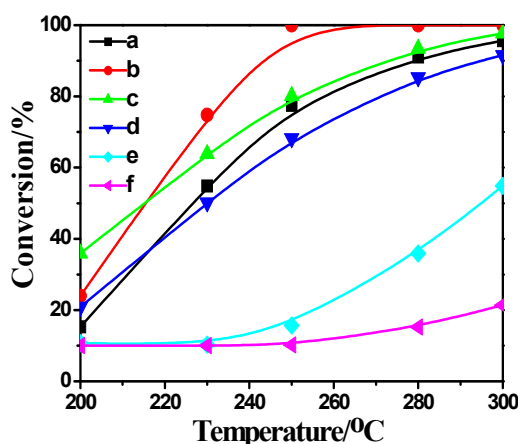


Figure 7. Activity measurement results of N_2O direct dissociation over $\text{Mg}_x\text{Ce}_y\text{Co}_{1-x-y}\text{Co}_2\text{O}_4$ ($x = 0.015, 0.025, 0.05, 0.1, 0.15$; $y = 0.05$) composite spinel metal-oxide catalysts. Reaction conditions: $\text{N}_2\text{O}:\text{He} = 35:65$, $\text{GHSV} = 30,000 \text{ h}^{-1}$; (a) $\text{Mg}_{0.015}\text{Ce}_{0.05}\text{Co}_{0.935}\text{Co}_2\text{O}_4$; (b) $\text{Mg}_{0.025}\text{Ce}_{0.05}\text{Co}_{0.925}\text{Co}_2\text{O}_4$; (c) $\text{Mg}_{0.05}\text{Ce}_{0.05}\text{Co}_{0.9}\text{Co}_2\text{O}_4$; (d) $\text{Mg}_{0.1}\text{Ce}_{0.05}\text{Co}_{0.85}\text{Co}_2\text{O}_4$; (e) $\text{Mg}_{0.15}\text{Ce}_{0.05}\text{Co}_{0.8}\text{Co}_2\text{O}_4$; (f) Co_3O_4 .

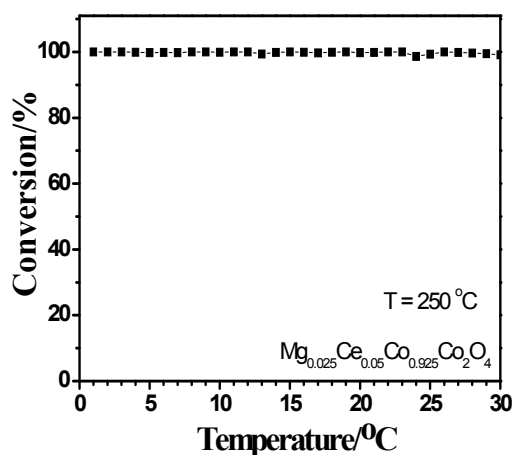


Figure 8. Long lifetime (30 h) activity measurement of N_2O direct dissociation over $Mg_{0.025}Ce_{0.05}Co_{0.925}Co_2O_4$ at $T = 250$ °C. Reaction conditions: $N_2O:He = 35:65$, $GHSV = 30,000$ h^{-1} .

2.5. Correlation between Characterization and Activity Measurement Result

In order to investigate Mg-, Ce-doping effects on the catalytic performance of Co_3O_4 , various characterizations, including XRD, BET, H_2 -TPR, and XPS were conducted for the samples of single metal doping and Mg, Ce co-doping on Co_3O_4 ($Mg_{0.2}Co_{0.8}Co_2O_4$, $Ce_{0.05}Co_{0.95}Co_2O_4$). As revealed by XRD and BET, Mg-, Ce-doping could reduce the grain size of Co_3O_4 , which in turn efficiently increases the related BET specific surface area: Co_3O_4 (32.5 $m^2 \cdot g^{-1}$) < $Mg_{0.2}Co_{0.8}Co_2O_4$ (77.8 $m^2 \cdot g^{-1}$) < $Ce_{0.05}Co_{0.95}Co_2O_4$ (106.5 $m^2 \cdot g^{-1}$) < $Mg_{0.025}Ce_{0.05}Co_{0.925}Co_2O_4$ (111.2 $m^2 \cdot g^{-1}$). Therefore, the highest specific surface of $Mg_{0.025}Ce_{0.05}Co_{0.925}Co_2O_4$ constitutes one of the important factors that led to the highest deN_2O activity. In addition to that, the improved redox abilities of Mg-, Ce-doped Co_3O_4 samples were observed based on H_2 -TPR, and these also play an important role during N_2O direct dissociation: (i) single Mg-doping could increase Co^{2+} content on $Mg_{0.2}Co_{0.8}Co_2O_4$; (ii) single Ce-doping could improve Co^{2+} redox ability; (iii) Mg-, Ce-doping could improve both Co^{3+} and Co^{2+} redox ability; (iv) compared with other Me-, Ce-doped Co_3O_4 samples, the highest redox ability of $Mg_{0.2}Co_{0.8}Co_2O_4$ is another reason for its showing the highest deN_2O activity. The XPS, utilized to investigate the surface atomic component and valence state, suggested that Mg-, Ce-doping did not influence the valence status of Co. However, the O1s suggested that Mg-, Ce-doping could efficiently enhance the mobility as well as content of surface atomic O, which is favorable for N_2O dissociation. Therefore, the highest mobility as well as content of surface atomic O on $Mg_{0.2}Co_{0.8}Co_2O_4$ constituted another important factor of its displaying the highest deN_2O . In summary, the highest BET specific surface area, redox ability, surface atomic O mobility, as well as surface oxygen content of the prepared Mg, Ce co-doped Co_3O_4 ($Mg_{0.025}Ce_{0.05}Co_{0.925}Co_2O_4$) constitute the main reasons for this sample having the highest deN_2O activity, which also make this kind of catalyst promising for further practical applications.

3. Experimental

3.1. Preparation of Catalyst

The composite spinel metal oxide catalysts of the present work ($Mg_xCo_{1-x}Co_2O_4$, $Ce_xCo_{1-x}Co_2O_4$, and $Mg_xCe_yCo_{1-x-y}Co_2O_4$) were prepared by a coprecipitation method. Firstly, a certain amount of metal nitrate solutions (magnesium nitrate, cerium nitrate, cobalt nitrate) were mixed together and placed in a 70 °C water bath, which was stirred for 20 min. Then, an appropriate amount of Na_2CO_3 was dissolved into 20 mL deionized water in a 70 °C water bath, which was stirred for 20 min. The above two solutions were mixed and the pH value was adjusted to 9. After filtration, drying (120 °C for 2 h), and calcination (400 °C for 3 h), the final catalyst samples were obtained.

3.2. Characterization of Catalysts

The XRD patterns of the prepared samples have been recorded in 2θ ranges from 5° to 80° , based on X-ray diffractometer (Rigaku, Tokyo, Japan, D/max2500VB2) and with a radiation of Cu $K\alpha$ ($\lambda = 1.5406 \text{ \AA}$). The crystal phases were confirmed according to the JCPDS reference. The crystallite sizes were calculated according to the Scherrer equation (Equation (3)) [3]. In this formula, K is Scherrer constant; β is the half width of the diffraction peak; and θ is a diffraction angle.

$$D = \frac{K\lambda}{\beta \cos \theta} \quad (3)$$

The specific surface area (S_{BET}) of the prepared catalyst sample was measured via a Sorptomatic 1990 instrument (Thermo Electron, Waltham, MA, USA) through nitrogen adsorption/desorption at 77 K and was calculated by the BET method. H_2 -TPR was performed using Thermo Electron TPD/R/O 1100 Series instrument equipped with a thermal conductivity detector (TCD). Before the experiment, samples were in turn pretreated by the following procedures: (1) heated at 100°C for 1 h in a He ($>99.999\%$) stream; (2) cooled down to 30°C under above atmosphere; (3) H_2 -TPR started with a ramp of $10^\circ\text{C}/\text{min}$ from 30 to 750°C . The flow rate of reducing gas (5.06% H_2 balanced by N_2) was 30 mL/min. XPS was conducted on a Thermo Fisher ESCALAB 250 system (Thermo Fisher Scientific, Waltham, MA, USA) with Al $K\alpha$ radiation under ultrahigh vacuum (UHV), calibrated internally by carbon deposit C (1s) having a binding energy (BE) of 284.6 eV.

3.3. Activity Measurement

N_2O direct decomposition was conducted in a fixed bed quartz tube reactor ($\Phi 7 \times 1 \times \text{L}300 \text{ mm}$) under atmospheric pressure. Pelletized catalyst (0.2 g) with particle sizes of 250–425 μm was placed in the constant temperature zone of a vertical tubular reactor. Afterwards, a gas mixture consisting of 35 vol % N_2O balanced by 65 vol % He was made according to the components of tail gas from related industrial plants as previously described [3] and fed into the reactor under atmospheric pressure. A total flow rate of 140 mL/min was employed for the activity test, corresponding to a GHSV (gas hourly space velocity) of $30,000 \text{ h}^{-1}$. The gaseous products were discontinuously analyzed by gas chromatograph (GC-4000A, Dongxi Co. Ltd., Beijing, China) equipped with a TCD and a TDX-01 column for the separation of N_2O , N_2 , and O_2 . The N_2O conversion was designed as follows:

$$\text{Conversion of } \text{N}_2\text{O} (\%) = 1 - \frac{[\text{N}_2\text{O}]}{[\text{N}_2\text{O}] + [\text{N}_2]} \times 100\% \quad (4)$$

where $[\text{N}_2\text{O}]$ and $[\text{N}_2]$ are the concentration of N_2O and N_2 , respectively, as measured by the chromatograph. Additionally, the outlet gases of the reactor were further analyzed a five-way gas analyzer (SIEMENS VS5067-5D). This analyzer has an infrared optical sensor and is able to detect NO, CO, CO_2 , O_2 , and hydrocarbons (HCs). The detection result suggested that N_2O was directly decomposed into N_2 and O_2 without generation of NO_x over the investigated samples.

4. Conclusions

In the present work, a series of Mg-, Ce-doped Co_3O_4 composite spinel metal-oxide catalysts was prepared and evaluated for N_2O direct dissociation. It was found that the Mg, Co co-doped Co_3O_4 with an optimum Mg/Ce mole ratio of 0.5 ($\text{Mg}_{0.025}\text{Ce}_{0.05}\text{Co}_{0.925}\text{Co}_2\text{O}_4$) exhibited the highest N_2O conversion activity, which could achieve 100% N_2O conversion at $T = 250^\circ\text{C}$. Various characterizations using XRD, BET, H_2 -TPR, and XPS were conducted to gain deeper insight into the Mg-, Ce-doping effect. Three main factors were found to contribute to the $\text{Mg}_{0.025}\text{Ce}_{0.05}\text{Co}_{0.925}\text{Co}_2\text{O}_4$ sample obtaining the highest $de\text{N}_2\text{O}$ activity: (a) Mg and Ce co-doping could reduce the grain size of composite spinel metal oxide, resulting in a significant increase of the BET specific surface area from $32.5 \text{ g}\cdot\text{m}^{-2}$ of pure Co_3O_4 to $111.2 \text{ g}\cdot\text{m}^{-2}$; (b) Mg and Ce co-doping could improve the redox ability of both $\text{Co}^{3+} \rightarrow \text{Co}^{2+}$

and $\text{Co}^{2+} \rightarrow \text{Co}^{2+}$; (c) Mg and Ce co-doping could improve the mobility as well as the concentration of surface atomic O.

Acknowledgments: The authors thank the National Natural Science Foundation of China (No. 21477007, 21407007, and Major Program 91534201), Natural Science Foundation of Jiangsu Province of China (No. BK20140268), the Fundamental Research Funds for the Central Universities (YS1401), BUCT Fund for Disciplines Construction and Development (Project No. XK1504).

Author Contributions: R.Z. and N.L. conceived and designed the experiments; P.C. performed the experiments; N.L. and P.C. analyzed the data; R.Z. and Y. L. contributed reagents/materials/analysis tools; N.L. wrote the paper.

Conflicts of Interest: The authors declare no conflict of interest.

References

1. Trogler, W.C. Physical Properties and Mechanisms of Formation of Nitrous Oxide. *Coord. Chem. Rev.* **1999**, *187*, 303–327. [[CrossRef](#)]
2. Zhang, R.; Liu, N.; Lei, Z.; Chen, B. Selective Transformation of Various Nitrogen-Containing Exhaust Gases toward N_2 over Zeolite Catalysts. *Chem. Rev.* **2016**, *116*, 3658–3721. [[CrossRef](#)] [[PubMed](#)]
3. Chen, B.; Liu, N.; Liu, X.; Zhang, R.; Li, Y.; Li, Y.; Sun, X. Study on the Direct Decomposition of Nitrous Oxide over Fe-Beta Zeolites: From Experiment to Theory. *Catal. Today* **2011**, *175*, 245–255. [[CrossRef](#)]
4. Liu, N.; Zhang, R.; Chen, B.; Li, Y.; Li, Y. Comparative Study on the Direct Decomposition of Nitrous Oxide over M(Fe, Co, Cu)-BEA Zeolites. *J. Catal.* **2012**, *294*, 99–112. [[CrossRef](#)]
5. Centi, G.; Perathoner, S.; Vazzana, F.; Marclla, M.; Tomaselli, M.; Mantegazza, M. Novel Catalysts and Catalytic Technologies for N_2O Removal from Industrial Emissions Containing O_2 , H_2O and SO_2 . *Adv. Environ. Res.* **2000**, *4*, 325–338. [[CrossRef](#)]
6. Galle, M.; Agar, D.W.; Watzenberger, O. Thermal N_2O Decomposition in Regenerative Heat Exchanger Reactors. *Chem. Eng. Sci.* **2001**, *56*, 1587–1595. [[CrossRef](#)]
7. Xia, H.; Sun, K.; Liu, Z.; Feng, Z.; Ying, P.; Li, C. The Promotional Effect of NO on N_2O Decomposition over the Bi-Nuclear Fe Sites in Fe/ZSM-5. *J. Catal.* **2010**, *270*, 103–109. [[CrossRef](#)]
8. Melian-Cabrera, I.; Mentrui, C.; Pieterse, J.A.Z.; van den Brink, R.W.; Mul, G.; Kapteijn, F.; Moulijn, J.A. Highly Active and Stable Ion-Exchanged Fe-Ferrierite Catalyst for N_2O Decomposition under Nitric Acid Tail Gas Conditions. *Catal. Commun.* **2005**, *6*, 301–305. [[CrossRef](#)]
9. Kameoka, S.; Suzuki, T.; Yuzaki, K.; Takeda, T.; Tanaka, S.; Ito, S.; Kunimori, K.; Miyadera, T. Selective Catalytic Reduction of N_2O with Methane in the Presence of Excess Oxygen over Fe-BEA Zeolite. *Chem. Commun.* **2000**, *9*, 745–746. [[CrossRef](#)]
10. Dacquín, J.P.; Dujardin, C.; Granger, P. Surface Reconstruction of Supported Pd on LaCoO_3 : Consequences on the Catalytic Properties in the Decomposition of N_2O . *J. Catal.* **2008**, *253*, 37–49. [[CrossRef](#)]
11. Franken, T.; Palkovits, R. Investigation of Potassium Doped Mixed Spinels $\text{Cu}_x\text{Co}_{3-x}\text{O}_4$ as Catalysts for an Efficient N_2O Decomposition in Real Reaction Conditions. *Appl. Catal. B* **2015**, *176–177*, 298–305. [[CrossRef](#)]
12. Zabitskiy, M.; Djinić, P.; Tchernychova, E.; Pintar, A. N_2O Decomposition over CuO/CeO_2 Catalyst: New Insights into Reaction Mechanism and Inhibiting Action of H_2O and NO by Operando Techniques. *Appl. Catal. B* **2016**, *197*, 146–158. [[CrossRef](#)]
13. Xue, L.; Zhang, C.; He, H.; Teraoka, Y. Catalytic Decomposition of N_2O over CeO_2 Promoted Co_3O_4 Spinel Catalyst. *Appl. Catal. B* **2007**, *75*, 167–174. [[CrossRef](#)]
14. Grzybeka, G.; Stelmachowska, P.; Gudykaa, S.; Indykaa, P.; Sojkaa, Z.; Guillén-Hurtadob, N.; Rico-Pérezb, V.; Bueno-Lópezb, A.; Kotarbaa, A. Strong Dispersion Effect of Cobalt Spinel Active Phase Spread over Ceria for Catalytic N_2O Decomposition: The Role of the Interface Periphery. *Appl. Catal. B* **2016**, *180*, 622–629. [[CrossRef](#)]
15. Stelmachowski, P.; Maniak, G.; Kaczmarczyk, J.; Zasada, F.; Piskorz, W.; Kotarba, A.; Sojka, Z. Mg and Al Substituted Cobalt Spinels as Catalysts for Low Temperature N_2O -Evidence for Octahedral Cobalt Active Sites. *Appl. Catal. B* **2014**, *146*, 105–111. [[CrossRef](#)]
16. Zhang, R.; Hedjazi, K.; Chen, B.; Li, Y.; Lei, Z.; Liu, N. M(Fe, Co)-BEA Washcoated Honeycomb Cordierite for N_2O Direct Decomposition. *Catal. Today* **2016**, *273*, 273–285. [[CrossRef](#)]
17. Liu, N.; Zhang, R.; Li, Y.; Chen, B. Local Electric Field Effect of TMI (Fe, Co, Cu)-BEA on N_2O Direct Dissociation. *J. Phys. Chem. C* **2014**, *118*, 10944–10956. [[CrossRef](#)]

18. Liu, N.; Chen, B.; Li, Y.; Zhang, R.; Liang, X.; Lei, Z. Charge Transfer Analysis on the Direct Decomposition of Nitrous Oxide over Fe-BEA Zeolite: An Experimental and Density Functional Study. *J. Phys. Chem. C* **2011**, *115*, 12883–12890. [[CrossRef](#)]
19. Watanabe, S.; Ma, X.; Song, C. Characterization of Structural and Surface Properties of Nanocrystalline TiO₂-CeO₂ Mixed Oxides by XRD, XPS, TPR, and TPD. *J. Phys. Chem. C* **2009**, *113*, 14249–14257. [[CrossRef](#)]
20. Li, X.; Hong, H. Co-M (*M* = La, Ce, Fe, Mn, Cu, Cr) Catalytic Decomposition of Complex Metal Oxides N₂O. *Acta Phys. Chim. Sin.* **2007**, *23*, 664–670.
21. Harrison, P.G.; Ball, I.K.; Daniell, W.; Lukinskas, P.; Céspedes, M.; Miró, E.E.; Ulla, M.A. Cobalt Catalysts for the Oxidation of Diesel Soot Particulate. *Chem. Eng. J.* **2003**, *95*, 47–55. [[CrossRef](#)]
22. Bahlawane, N.; Rivera, E.F.; Kohse-Höinghaus, K.; Brechling, A.; Kleineberg, U. Characterization and Tests of Planar Co₃O₄ Model Catalysts Prepared by Chemical Vapor Deposition. *Appl. Catal. B* **2004**, *53*, 245–255. [[CrossRef](#)]
23. Karlsen, E.J.; Nygren, M.A.; Pettersson, L.G.M. Theoretical Study on the Decomposition of N₂O over Alkaline Earth Metal-Oxides: MgO-BaO. *Phys. Chem. A* **2002**, *106*, 41–50. [[CrossRef](#)]
24. He, H. Influence of Alkaline Earth Metals on Cobalt-Cerium Composite Oxide Catalysts for NO Decomposition. *Acta Phys. Chim. Sin.* **2009**, *25*, 1033–1039.
25. Huang, T.J.; Wang, C.H. Roles of Surface and Bulk Lattice Oxygen in Forming CO₂ and CO during Methane Reaction over Gadolinia-Doped Ceria. *Catal. Lett.* **2007**, *118*, 103–108. [[CrossRef](#)]



© 2017 by the authors; licensee MDPI, Basel, Switzerland. This article is an open access article distributed under the terms and conditions of the Creative Commons Attribution (CC-BY) license (<http://creativecommons.org/licenses/by/4.0/>).